Journal of Photochemistry and Photobiology A: Chemistry 226 (2011) 9–15

Contents lists available at SciVerse ScienceDirect

Journal of Photochemistry and Photobiology A: Chemistry

journal homepage: www.elsevier.com/locate/jphotochem

A compact diketopyrrolopyrrole dye as efficient sensitizer in titanium dioxide dye-sensitized solar cells

Julien Warnan, Ludovic Favereau, Yann Pellegrin, Errol Blart, Denis Jacquemin*, Fabrice Odobel*

Université de Nantes, CNRS, Chimie et Interdisciplinarité: Synthèse, Analyse, Modélisation (CEISAM), UMR CNRS n° 6230, 2, rue de la Houssinière – BP 92208 – 44322 Nantes Cedex 3, France

ARTICLE INFO

Article history:
Received 20 August 2011
Accepted 24 September 2011
Available online 14 October 2011

Keywords:
Dye-sensitized solar cells
Organic sensitizers
TiO_2
TD-DFT calculations
Diketopyrrolopyrrole

ABSTRACT

Two novel TiO_2 sensitizers, based on the highly stable diketopyrrolopyrrole (DPP) skeleton, have been synthesized for application in the field of dye sensitized solar cells. The obtained dyes, **DPP1** and **DPP2** bear respectively a cyanoacrylic acid and a rhodanine acid anchoring groups, thus tuning the extent of the electronic communication with the semi-conducting oxide. The two chromophores were characterized by solution phase spectroscopy and electrochemistry. DFT calculations gave deeper insight into the electronic structure of both dyes, through the disclosure of their frontier orbitals. Photovoltaic performances unravelled the undisputable advantage of **DPP1** over **DPP2**, owing to the combination of a favourable dipolar moment interaction with TiO_2, and more intimate orbital blending between the chemisorbed dye and the conduction band. Chenodeoxycholic acid proved to be useful in limiting the formation of dye aggregates, improving to a great extent the performances of **DPP1** based DSSCs, reaching in our conditions a 4.47% yield and 57% IPCE at 500 nm.

1. Introduction

Discovering efficient and robust organic sensitizers is an important goal in the field of dye-sensitized solar cell (DSSC) and has therefore stimulated countless investigations for more than a decade [1]. Originally, ruthenium polypyridine complexes were the dominating sensitizers used in this area [2] but since 2000 many classes of organic dyes were systematically investigated and some of them achieved impressive photo-conversion efficiencies around 10% and even higher [3–5]. Diketopyrrolopyrrole (DPP) is a well-known chromogen with particularly high photostability [6] and which was quite thoroughly used as electron donor unit in organic solar cells [7]. However, there are only three reports on the use of this class of dyes in DSSC [8,9]. For its outstanding photo-stability, high absorbance in the visible region, high synthetic accessibility, we felt that DDP derivatives could constitute efficient sensitizers for DSSC and deserved further investigations. In this study, we prepared two new compact dyes as we strive for obtaining a significant sensitizer efficiency with a minimal size. The two compounds essentially differ by their anchoring group: cyanoacrylic acid for DDP1 and rhodanine-3-acetic acid for **DPP2** (Chart 1).

To provide a good solubility of the dyes, the nitrogen of lactam units were alkylated by branched fatty alkyl chains. Moreover, these substituents could also wrap the dye core and limit their aggregation upon binding on the TiO_2 surface. They can also prevent the I_3^- from approaching the surface of TiO_2 and inhibit the interception of the injected electron by the electrolyte [5,10]. In spite of its simplicity, we demonstrate that **DPP1** clearly represents a valuable unit to prepare efficient diketopyrrolopyrrole-based sensitizers, since it gives the best photo-conversion efficiency reported for this class of dye [9].

2. Synthesis

Preparation of the DDP core follows a previously described method consisting in a pseudo-Stobbe condensation of 1-bromo-4-cyanobenzene and diethylsuccinate in presence of a strong base [11,12]. A double alkylation was subsequently achieved by deprotonation of the lactam units by potassium *tert*butanolate which was reacted with the branched alkyl 1-bromo-2-ethylhexane in *N*-methylpyrrolidone to furnish compound **1** in a modest yield of 26% [13]. Then, a Suzuki cross-coupling reaction with the 4-formylthiophenyl boronic acid in presence of sodium carbonate and tetrakis(triphenylphosphine)palladium as catalytic system led to the aldehyde **2** with a yield of 34% (Scheme 1) [9,11,14]. The two other main products were the starting material **1** and the bis-coupled product but they were easily separated by column chromatography due to their very different polarities. Finally, two

* Corresponding authors. Tel.: +33 02 51 12 54 29; fax: +33 02 51 12 54 02.
E-mail addresses: denis.jacquemin@univ-nantes.fr (D. Jacquemin), Fabrice.Odobel@univ-nantes.fr (F. Odobel).

1010-6030/$ – see front matter © 2011 Elsevier B.V. All rights reserved.
doi:10.1016/j.jphotochem.2011.09.023

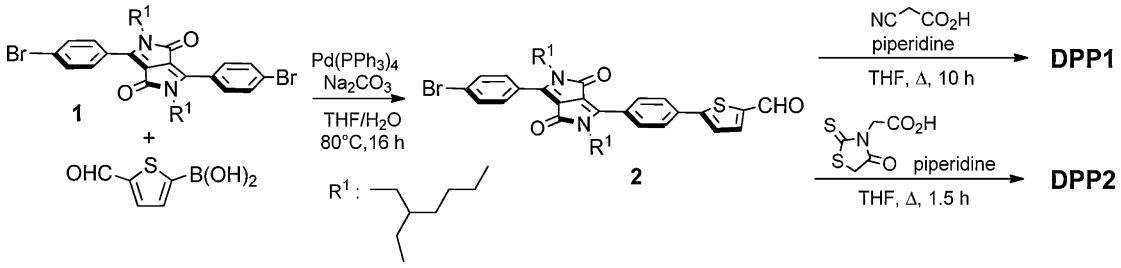

Scheme 1. Synthesis of **DPP1** and **DPP2**.

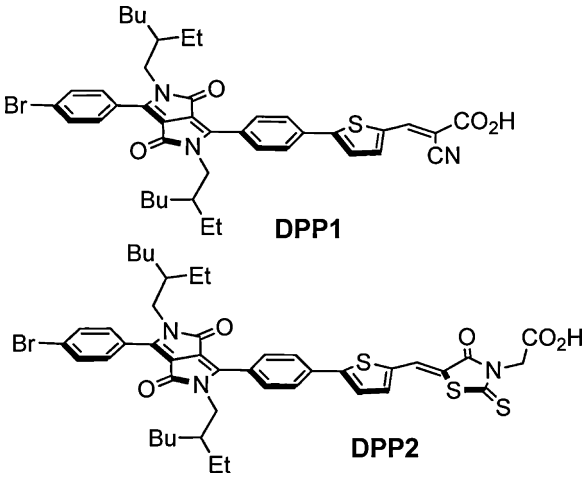

Chart 1. Structure of the dyes investigated in this study.

Knoevenagel reactions of compound **2** with cyanoacrilic acid or with rhodanine-3-acetic acid afforded respectively the final targets **DPP1** or **DPP2** with high yield (>95%).

3. Electronic absorption and emission spectra

The electronic absorption spectra of the two new dyes were recorded in dichloromethane solution and on TiO_2. The spectra are respectively illustrated in Figs. 1 and 2 and the data are collected in Table 1. Diketopyrrolopyrroles usually exhibit intense π–π^* transitions in the visible. In **DPP1** and **DPP2** the absorption bands around 400 and 500 nm are dominated by a HOMO–LUMO and (HOMO−1) – LUMO/HOMO – (LUMO+1) contributions, respectively (see below QM calculations). These transitions correspond to a partial charge transfer (CT), in which the electron density shifts from the DPP core towards the anchoring moiety. On TiO_2, the spectral coverage spans from 380 nm to 600 nm, with a shallower valley around 450 nm and slightly larger absorption window for **DPP2** (Fig. 2). The presence of chenodeoxycholic acid (CDCA) during the chemisorption step induces a small but noticeable blue-shift of the absorption spectra (Fig. 2). This supports the fact that CDCA certainly prevents the formation of aggregates of these dyes on TiO_2, though aggregation was originally very limited, thanks to, the alkyl chains on the lactam units. **DPP1** and **DPP2** are both strongly fluorescent molecules and they display a strong emission band around 650 nm, which gives a singlet excited state lying at about 2.25 eV (Fig. 1 and Table 1).

4. Electrochemistry

The redox potentials of the dyes were recorded by cyclic voltammetry to assess the thermodynamic feasibilities of the electron transfer processes. Both dyes exhibit a reversible oxidation at around 1.2 V vs. SCE with marginal influence of the anchoring group which is consistent with the topology of the HOMO orbital. Indeed, the latter is rather localized on the DPP unit with almost no contribution of the anchoring group (Fig. 3). Using the well-accepted values of −0.5 V vs. NHE [15] (−0.74 V vs. SCE) for the conduction band of TiO_2 and of 0.40 V vs. NHE [16] (0.16 V vs. SCE) for the redox couple $I_2^{\bullet-}/I^-$, the electron injection Gibbs free energy (ΔG_{inj}) and the dye regeneration Gibbs free energy (ΔG_{reg}) have been calculated (Table 1). Clearly, the electron injection driving force (ΔG_{inj}) is relatively weak leaving the possibility of a sluggish reaction for both dyes while the regeneration reaction of the oxidized sensitizer ($S^+ + 2I^- \rightarrow S + I_2^{\bullet}$) is highly favourable ($\Delta G_{reg} < -1$ eV) in both cases (Table 1).

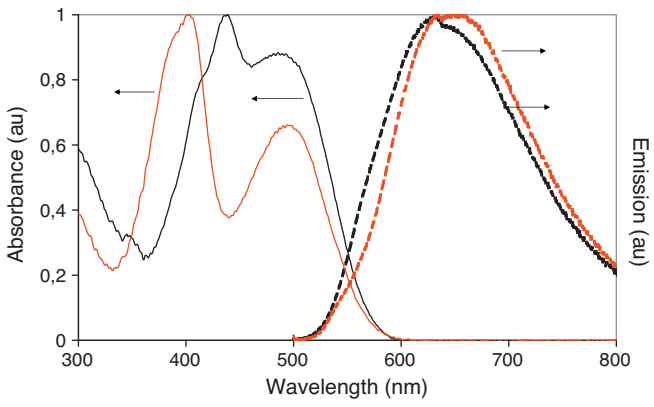

Fig. 1. Normalized absorption (straight line) spectra and emission (dashed line) of **DPP1** (red) and **DPP2** (black) recorded in dichloromethane. (For interpretation of the references to color in this figure legend, the reader is referred to the web version of this article.)

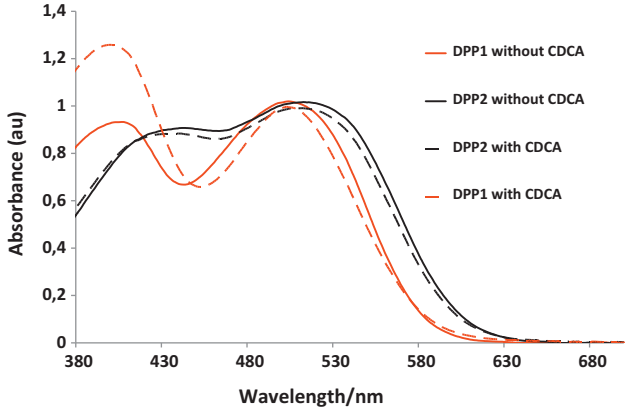

Fig. 2. Normalized absorption spectra of **DPP1** (red) and **DPP2** (black) recorded TiO_2 electrodes with chenodeoxycholic acid (straight line) and without (dashed line). (For interpretation of the references to color in this figure legend, the reader is referred to the web version of this article.)

Table 1
Absorption and emission characteristics along with redox potential and injection Gibbs free energies of **DPP1** and **DPP2**.

Dye	$E_{Ox}(S^+/S)$ V vs. SCE	$\lambda_{abs}/\varepsilon$(nm/M^{-1}cm^{-1})	λ_{em} (nm)	[a] $E_{00}(S^*)$ (eV)	[b] $E_{Ox}(S^+/S^*)$ V vs. SCE	[c] ΔG_{inj} (eV)	[d] ΔG_{reg} (eV)
DPP1	1.20	403 (2.1×10^4); 493 (1.4×10^4)	653	2.24	−1.04	−0.30	−1.04
DPP2	1.18	416 (1.3×10^4); 503 (1.2×10^4)	641	2.25	−1.07	−0.33	.1.02

SCE, saturated calomel electrode.
[a] Calculated with the wavelength at the intersection (λ_{inter}) normalized absorption and emission spectra with the equation $E_{00} = 1240/\lambda_{inter}$.
[b] Calculated according to the equation: $E_{Ox}(S^+/S^*) = E_{Ox}(S^+/S) - E_{00}$.
[c] Calculated according to the equation: $\Delta G_{inj} = 0.74 + E_{Ox}(S^+/S^*)$.
[d] Calculated according to the equation: $\Delta G_{reg} = 0.16 - E_{Ox}(S^+/S)$.

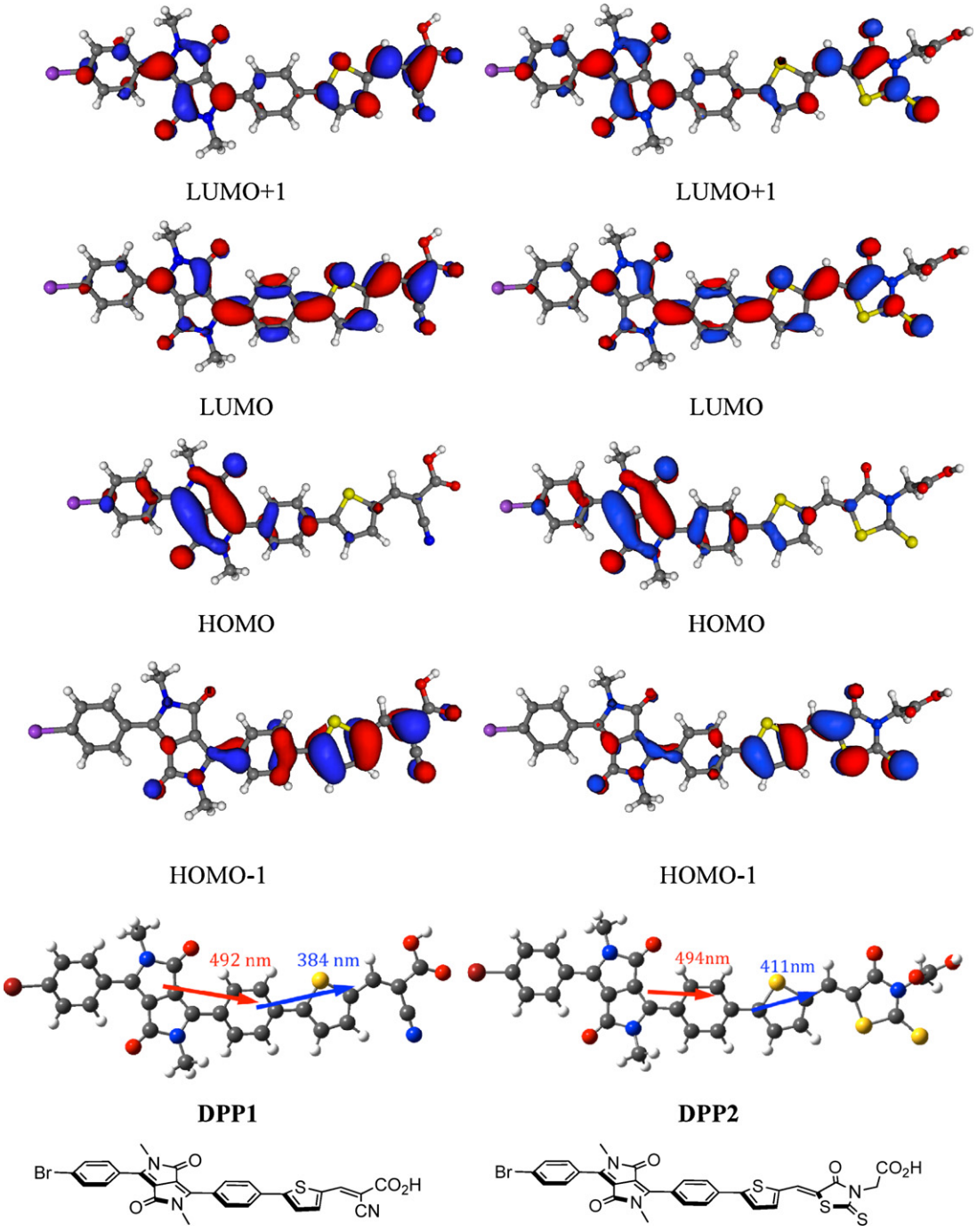

Fig. 3. Graphical representation of the optimized structure with representation of CT of both absorption bands (see text) and of the frontier molecular orbitals of **DPP1** (left) and **DPP2** (right). Branched alkyl chains were replaced by methyl groups for faster calculations.

5. Quantum chemical calculations

The structural parameters of both dyes have been optimized using Density Functional Theory (see section 10 for details), and have been found to be nearly planar, e.g. for **DPP1** the twist angles between the diketopyrrolopyrrole moiety and the side phenyl rings are *ca.* 30°, whereas the phenyl-thiophene dihedral angle is 21°. In order to get insight into the electronic structure, Time-Dependent DFT (TD-DFT) calculations were performed on both dyes. For **DPP1** (**DPP2**), we compute two strongly dipole-allowed transitions in the visible, at 492 and 384 nm (494 and 411 nm), which fits experiments (Fig. 1), including the significant bathochromic shift of the second band when going from **DPP1** to **DPP2**. The TD-DFT fluorescence wavelengths from the lowest excited-states are 648 and 650 nm for **DPP1** and **DPP2** and also nicely match with the experimental values. The excited-state geometry is significantly more planar (e.g. phenyl-thiophene dihedral angle of 0.2° for **DPP1**) than the ground state, which partly explains the significant Stokes shift. For both dyes, the *ca.* 490 nm absorption band is dominated by an HOMO–LUMO transition but also includes a smaller HOMO–LUMO+1 component, whereas the *ca.* 400 nm absorption includes almost equal shares of HOMO−1–LUMO and HOMO–LUMO+1 contributions. These frontier molecular orbitals are shown in Fig. 3. We observe that the methylene carboxylic acid moiety of rhodanine-3-acetic acid anchoring group in **DPP2** orients perpendicularly to the rest of the molecule. On the contrary, **DPP1** is a relatively planar dye, which ensures a high degree of π-conjugation throughout the molecule. In both dyes, the electron density on HOMO is located on the diketopyrrolopyrrole core and particularly on the double bonds and the oxygen of the lactam units. The LUMO and LUMO+1 are distributed on the anchoring group and spreads up to the carboxylic acid group for **DPP1**, whereas in **DPP2** there is no contribution on the carboxylic acid group in **DPP2** there is no contribution on the carboxylic acid group. Another way to qualitatively account for the importance of electron transfer is to estimate the CT vector, as recently suggested by Ciofini and co-workers [17]. For both absorption bands, the CT distance is found to be significantly smaller for **DPP2** (*ca.* 3.5 Å) than for **DPP1** (*ca.* 4.7 Å), as illustrated at the bottom of Fig. 3. As a result, **DPP1** certainly features a much higher electronic communication between **DPP1** and with the conduction band of TiO_2 combined to a stronger CT character, hence a higher electronic coupling and a faster electron injection reaction with **DPP1** than with **DPP2**. Another striking difference between **DPP1** and **DPP2** is their ground-state dipole moments, which are estimated to 10.4 D and 4.9 D, respectively. It is therefore likely that **DPP1** induces a larger bending of the conduction band than **DPP2**, a factor, which was previously attributed to have an impact on the V_{oc} [18].

6. Photovoltaic measurements

Both dyes **DPP1** and **DPP2** were tested in DSSC and the data are collated in Table 2 and incident photon-to-current conversion efficiency (IPCE) spectra are depicted in Fig. 4. In these experiments, we used the classical iodide/triiodide electrolyte composed of 0.6 M 1,2-dimethyl-3-butylimidazolium iodide, 0.1 M LiI and 0.05 M I_2 in acetonitrile and we also tested the influence on the photovoltaic performances of 4-*tert*-butylpyridine additive (0.5 M) and of chenodeoxycholic acid (CDCA) as co-adsorbate. First, we observe that CDCA significantly improves the photocurrent density of **DPP1**, which passes from 7.78 to 9.71 mA/cm^2 whereas it has a detrimental impact on **DPP2**, whose photocurrent dropped upon CDCA co-adsorption. The effects of CDCA are two folds. First, it reduces dye aggregation but at the cost of a lower loading of the sensitizer on the TiO_2, because the surface occupation is shared with two different molecules instead of one. Second, the proton release during the chemisorption step acidifies the TiO_2 surface and induces a downward bending of the conduction band [19]. This latter effect is certainly important here as both dyes display rather low injection driving force (Table 1). Therefore, upon band bending the exergonicity of the charge injection is increased which enhances the photocurrent density. This beneficial effect is only observed with **DPP1**, because **DPP2** exhibits a poor electronic coupling, therefore the slight increase of the injection driving force is counter-balanced by the lower dye loading. The 4-*tert*-butylpyridine also plays two roles. On the one hand, it binds to the TiO_2 surface and causes an upward conduction band bending; on the other hand it prevents close contact between the TiO_2 surface and triiodide, subsequently reducing current losses by recombination. These two effects essentially raise the V_{oc}. Not surprisingly, the presence of 4-*tert*-butylpyridine increases the V_{oc}, but importantly decreases the overall photovoltaic performances of both **DPP1** and **DPP2** by dramatically diminishing the J_{sc}, which is the direct consequence of the already low injection Gibbs free energy, a feature that is exacerbated by the upward bending of the conduction band. The very large difference of power conversion efficiencies of **DPP1**, anchored with cyanoacrylic group, compared to that of **DPP2** linked to TiO_2 *via* rhodanine-3-acetic acid is quite impressive (Table 2 and Fig. 4). This is the direct consequence of the lower electronic coupling with **DPP2** due to the presence of a methylene unit in rhodanine-3-acetic acid, which interrupts the π-conjugation between the dye and TiO_2 and slows down charge injection. Recently, it was also proposed that cyanoacrylic acid injects electrons more deeply into the bulk of TiO_2, while with rhodanine-3-acetic acid the electron resides in the surface at a shorter distance than from the oxidized dye supporting thus a higher probability of charge back recombination [20]. Another interesting difference is the higher V_{oc} measured with **DPP1** (V_{oc} = 625 mV) than with **DPP2** (V_{oc} = 485 mV). It probably results from the higher dipolar moment of **DPP1** which

Table 2
Photovoltaic performances for **DPP1** and **DPP2** cell in response to 100 mW/cm^2 illumination.

Dye	CDCA	t-BuPy	V_{oc} (mV)	J_{sc} (mA/cm^2)	ff (%)	η(%)
DPP1	No	No	605	7.78	70.7	3.33
		Yes	615	2.17	73.8	0.99
	Yes	No	625	9.71	73.7	4.47
		Yes	635	3.09	79.2	1.55
DPP2	No	No	475	1.72	76.6	0.63
		Yes	525	0.37	68.5	0.13
	Yes	No	485	1.30	70.1	0.44
		Yes	525	0.44	71.8	0.16

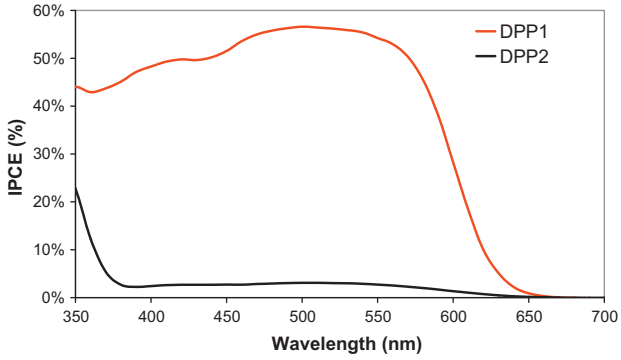

Fig. 4. Photoaction spectra of **DPP1** and **DPP2** co-adsorbed with CDCA and in absence of *tert*-butylpyridine in the electrolyte.

bends more significantly the TiO_2 conduction band than **DPP2** and consequently raises the V_{oc}. Anyhow to the best of our knowledge, **DPP1** is the most efficient sensitizer based on the diketopyrrolopyrrole chromogen. Indeed, in our conditions, it exhibits a J_{sc} = 9.71 mA/cm^2, a V_{oc} = 625 mV and a ff = 73.7% corresponding to a η of 4.47% with an IPCE curve demonstrating a continuous electricity production from 400 to −600 nm (Fig. 4).

7. Conclusions

In this work, we prepared and characterized two new compact diketopyrrolopyrrole dyes that are efficient sensitizers for TiO_2 DSSC. We showed that **DPP1** bearing a cyanoacrylic acid anchoring group is far superior to **DPP2** with a rhodanine-3-acetic acid group. This highlights the strong influence of the anchoring group on the photovoltaic performances, which becomes critical when the electron injection driving force is moderate. **DPP1** constitutes a suitable molecular building block to engineer more efficient diketopyrrolopyrrole-based sensitizer for DSSC. To improve the above systems, it will be necessary to enlarge the electron injection driving force. This study provides valuable guidelines for optimizing diketopyrrolopyrrole-based sensitizer for DSSC.

8. Experimental part

^{1}H and ^{13}C NMR spectra were recorded on a Bruker ARX 300 MHz. Chemical shifts for ^{1}H NMR spectra are referenced relative to residual protium in the deuterated solvent ($CDCl_3$ δ = 7.26 ppm for ^{1}H and δ = 77.16 ppm for ^{13}C; THF-d8 δ = 3.57, 1.72 ppm for ^{1}H). Spectra were recorded at room temperature, chemical shifts are written in ppm and coupling constants in Hz. MALDI-TOF analyses were performed on a *Bruker Ultraflex III*, microTOF Q spectrometer in positive linear mode at 20 kV acceleration voltage with 2,5-dihydroxybenzoic acid (DHB) or dithranol as matrix. Electrochemical measurements were performed with a potentiostat-galvanostat *AutoLab PGSTAT 302N* controlled by resident GPES software (General Purpose Electrochemical System 4.9) using a conventional single-compartment three-electrode cell. The working electrode was a Pt electrode, the auxiliary was a Pt wire of 10 mm long and the reference electrode was the saturated potassium chloride calomel electrode (SCE). The supporting electrolyte was 0.1 N Bu_4NPF_6 in CH_2Cl_2 and solutions were purged with argon before the measurements. All potentials are quoted relative to SCE. In all the experiments the scan rate was 100 mV/s. UV–Visible absorption spectra were recorded on a *UV-2401PC Shimadzu* spectrophotometer. Fluorescence spectra were recorded on a *SPEX Fluoromax* fluorimeter. Infrared spectra (IR) were recorded on a *BRUKER Vector 22* spectrometer; frequencies are reported in cm^{-1}.

Thin-layer chromatography (TLC) was performed on aluminium sheets precoated with Merck 5735 Kieselgel 60F_{254}. Column chromatography was carried out with Merck 5735 Kieselgel 60F (0.040–0.063 mm mesh). Chemicals were purchased from Sigma–Aldrich and used as received. Chenodeoxycholic acid and titanium dioxide screen printing pastes were purchased from Solaronix SA (Switzerland). Compound **1** was prepared according to literature methods [12,13].

8.1. Compound **2** (adapted procedure from previous publication [9])

Compounds **1** (3.0×10^{-4} mol), $Pd(PPh_3)_4$ (2.1×10^{-5} mol), and sodium carbonate (5.3×10^{-3} mol) were solubilised in 4 mL of THF + 2 mL of H_2O, underargon atmosphere. The blend was heated at 45 °C for 0.5 h, then a solution of 4-formylthiophenylboronic acid (3.4×10^{-4} mol) in 4 mL of THF was added. The temperature was increased to 80 °C and maintained for 16 h. Once back at room temperature, water was poured and the crude extracted with dichloromethane. After two aqueous washings, the organic phase was dried on $MgSO_4$, filtered and concentrated to give a red solid. The product was then purified on silicagel column chromatography with dichloromethane as eluent. A yellow ring corresponding to the starting material was collected first, followed by an orange fraction corresponding to pure compound **2** (1.0×10^{-4} mol, 34%). ^{1}H NMR (300 MHz, $CDCl_3$): δ_H = 9.91 (1H, s); 7.84 (2H, d, ^3J = 8.6); 7.76 (3H, m); 7.76 (2H, d, ^3J = 8.5); 7.62 (4H, bs); 7.48 (1H, d, ^3J = 4.0); 3.75 (2H, d, ^3J = 7.8), 3.71 (2H, d, ^3J = 7.6), 1.45 (2H, m), 1.08 (16H, m), 0.74 (12H, m). ^{13}C NMR (75 MHz, $CDCl_3$): δ_c = 182.9, 162.6, 152.7, 147.9, 143.4, 137.4, 135.4, 132.2, 130.2, 129.6, 129.2, 127.3, 126.7, 125.7, 125.2, 110.3, 110.2, 45.2, 45.1, 38.7, 30.4, 28.4, 23.9, 23.0, 14.1, 10.6. MALDI-TOF: *m*/*z*: Calcd for: 701.2407 [MH]$^+$, Found: 701.2419 [MH]$^+$, Δ = 1.7 ppm.

8.2. Compound ***DPP1***

Compound **2** (2.1×10^{-5} mol) and cyanoacrylic acid (6.4×10^{-4} mol) were placed in 4 mL of dry THF before distilled piperidine (9.0×10^{-4}) was added. The solution was heated to reflux for 10 h. The solution's colour turned to deep red and the degree of advancement was followed by TLC. At room temperature dichloromethane and a diluted solution of hydrochloric acid were added and the organic phase was washed with water and dried on Na_2SO_4. After filtration and concentration the crude was purified by silicagel column chromatography mounted with a mixture of dichloromethane and methanol (9/1). After the removal of low polarity residues, a few amounts of triethylamine were added to the eluent. The obtained red fraction was washed with a hydrochloric acid solution (1 M), dried, filtered and concentrated to furnish a red solid (96%). ^{1}H NMR (300 MHz, THF-d8): δ_H; 8.36 (1H, s); 7.96 (2H, d, ^3J = 8.4); 7.88 (3H, m); 7.76 (2H, d, ^3J = 8.5); 7.69 (1H, d, ^3J = 4.0); 7.63 (2H, d, ^3J = 8.5); 3.81 (2H, d, ^3J = 7.3), 3.77 (2H, d, ^3J = 7.5), 1.43 (2H, m), 1.11 (16H, m), 0.72 (12H, m) FT-IR (KBr, cm^{-1}): 2218, 1698, 1652, 1121. MALDI-TOF: *m*/*z*: Calcd for: 768.2465 [MH]$^+$, Found: 768.2438 [MH]$^+$, Δ = 3.5 ppm.

8.3. Compound ***DPP2***

Compound **2** (2.1×10^{-5} mol) and rhodanine-3-acetic acid (2.1×10^{-4} mol) were placed in 4 mL of dry THF before distilled piperidine (9.0×10^{-4}) was added. The solution was heated to reflux for 1.5 h. The solution's colour turned to deep red and the degree of advancement was followed by TLC. At room temperature dichloromethane and a diluted solution of hydrochloric acid were added before organic phase was washed with water and dried on Na_2SO_4. After filtration and concentration the crude was purified by silicagel column chromatography mounted with a mixture of dichloromethane and methanol (9/1). After elimination of low polarity residues, a few amounts of triethylamine were added to the solvent of chromatography. The obtained red fraction was washed with a hydrochloric acid solution (1 M), dried, filtered and concentrated to furnish a red solid (99%). ^{1}H NMR (300 MHz, THF-d8): δ_H = 8.11 (1H, s); 7.98 (2H, d, ^3J = 7.9); 7.90 (2H, d, ^3J = 7.9); 7.79 (2H, d, ^3J = 8.4); 7.71 (1H, d, ^3J = 4.0); 7.66 (2H, d, ^3J = 8.4); 7.61 (1H, d, ^3J = 3.9), 4.79 (2H, s), 3.83 (2H, d, ^3J = 7.0), 3.79 (2H, d, ^3J = 7.3), 1.43 (2H, m), 1.12 (16H, m), 0.75 (12H, m) MALDI-TOF: *m*/*z*: Calcd for: 873.1934 [MH]$^+$, Found: 873.1902 [MH]$^+$, Δ = 3.7 ppm.

9. Fabrication of the dye-sensitized solar cells

Conductive glass substrates (F-doped SnO_2) were purchased from Pilkington (TEC8, sheet resistance 8 Ω^{-2}). Conductive glass FTO substrates were successively cleaned by sonication in soapy water, then ethanol for 10 min before being fired at 450 °C for 30 min. Once cooled down to room temperature, FTO plates were rinsed with ethanol and dried in ambient air. TiO_2 films were then prepared in three steps. A first treatment is applied by immersion for 30 min in an aqueous $TiCl_4$ solution (50 mM) at 80 °C. Layers of TiO_2 were then screen printed with transparent colloidal paste Ti-Nanoxide T20/SP and light scattering Ti-Nanoxide 300 as final layer, with intermediate drying steps at 150 °C for 10 min between each layer. The obtained substrates were then sintered at 450 °C, following a progressive heating ramp (325 °C for 5 min, 375 °C for 5 min, 450 °C for 30 min). A second $TiCl_4$ treatment was applied while cells are still hot. Thicknesses were measured by a Sloan Dektak 3 profilometer. The prepared TiO_2 electrodes were soaked while still hot (80 °C) in a 0.16 mM solution of each dye during 16 h. A mixture of distilled solvents was used (dichloromethane/tetrahydrofuran 3/1, v/v) for bath preparation. In case of co-adsorption, required quantity of chenodeoxycholic acid (0.6 mM) was added to the bath before soaking.

Electrolytes used are composed of: 0.6 M 1,2-dimethyl-3-butylimidazolium iodide, 0.1 M LiI and 0.05 M I_2 in acetonitrile, with or without *t*-butylpyridine (0.5 M). Counter electrodes were prepared by chemical deposition of platinum from hexachloroplatinic acid in distilled isopropanol (2 mg/mL) and subsequent firing at 375 °C for 20 mn. The two electrodes were placed on top of each other using a thin transparent film of Surlyn polymer (DuPont, 25 μm) as a spacer to form the electrolyte space. The empty cell was tightly held, and the edges were heated to 110 °C to seal the two electrodes together. A drop of electrolyte was introduced through a predrilled hole in the counter electrode by vacuum backfilling, and was sealed afterwards. The cells have an active area of *ca.* 0.25 cm^2.

The current–voltage characteristics were determined by applying an external potential bias to the cell and measuring the photocurrent using a Keithley model 2400 digital source meter. The solar simulator is an Oriel Lamp calibrated to 100 mW/cm^2. The overall conversion efficiency (η) of the photovoltaic cell is calculated from the product of the photocurrent density (J_{sc}), the open-circuit photovoltage (V_{oc}), the fill factor of the cell (ff) divided by the intensity of the incident light (100 mW/cm^2).

10. Theoretical calculations

All simulations have been achieved with Gaussian09 program [21], applying default procedures, integration grids, algorithms and parameters, except for tighten SCF (10^{-9} a.u.) and internal forces (10^{-5} a.u.) convergence thresholds. We have adopted a three step strategy that is efficient to determine the UV/Vis features of most organic dyes [22]. The computational protocol systematically (all steps) includes a modelling of bulk solvent effects (here CH_2Cl_2) through the Polarizable Continuum Model (PCM) [23] and proceeds as: (1) the ground-state geometrical parameters have been determined at the PBE0/6-311G(d,p) level [24], *via* a force-minimization process; (2) the vibrational spectrum of each derivatives has been determined analytically at the same level of theory, that is PBE0/6-311G(d,p), and it has been checked that all structures correspond to true minima of the potential energy surface; (3) the first ten low-lying excited-states have been determined within the vertical TD-DFT approximation using the CAM-B3LYP/6-311+G(2d,p) level of approximation [25]; and (4) the fluorescence wavelengths were estimated though the use of vertical CAM-B3LYP/6-311 + G(2d,p) transition energies computed on the optimal PBE0/6-311G(d,p) geometries determined for the first excited-state though a PCM-TD-DFT optimization [26]. The contour threshold selected to represent the molecular orbitals was systematically set to 0.030 a.u. To estimate the charge-transfer, we have used the procedure defined by Ciofini and coworkers [17], but selected (Mulliken) partial atomic charges rather than electronic densities as starting data. For both dyes, the lateral alkyl chains, that are not expected to play a significant role in the optical properties and have been replaced by methyl groups (see Fig. 3) for the sake of computational efficiency.

Acknowledgements

The authors wish to thank the ANR HABISOL (program Asyscol, n° ANR-08-HABISOL-002) for financial support. D.J. is indebted to the *Région des Pays de la Loire* for financial support in the framework of a *recrutement sur poste stratégique*. This research used resources of the GENCI-CINES/IDRIS (Grant c2011085117) and of the CCIPL (*Centre de Calcul Intensif des Pays de Loire*).

References

[1] A. Mishra, M.K.R. Fischer, P. Bauerle, Angew. Chem. Int. Ed. 48 (2009) 2474.
[2] (a) A.S. Polo, M.K. Itokazu, N.Y. Murakami Iha, Coord. Chem. Rev. 248 (2004) 1343;
(b) B. O'Regan, M. Grätzel, Nature 353 (1991) 737;
(c) V. Yam, M. Nazeeruddin, M. Grätzel, Transition metal complexes for photovoltaic and light emitting applications, in: Photofunctional Transition Metal Complexes, Springer, Berlin/Heidelberg, 2007, pp. 113–123.
[3] (a) S. Ito, H. Miura, S. Uchida, M. Takata, K. Sumioka, P. Liska, P. Comte, P. Pechy, M. Gratzel, Chem. Commun. 5194 (2008);
(b) T. Bessho, S.M. Zakeeruddin, C.-Y. Yeh, E.W.-G. Diau, M. Graetzel, Angew, Chem. Int. Ed. 49 (2010) 6646.
[4] (a) W. Zeng, Y. Cao, Y. Bai, Y. Wang, Y. Shi, M. Zhang, F. Wang, C. Pan, P. Wang, Chem. Mater. 22, (2010) 1915;
(b) T. Horiuchi, H. Miura, K. Sumioka, S.J. Uchida, Am. Chem. Soc. 126 (2004) 12218.
[5] N. Koumura, Z.-S. Wang, S. Mori, M. Miyashita, E. Suzuki, K. Hara, J. Am. Chem. Soc. 128 (2006) 14256.
[6] (a) M. Fukuda, K. Kodama, H. Yamamoto, K. Mito, Dyes Pigments 63 (2004) 115;
(b) Z. Hao, A. Iqbal, Chem. Soc. Rev. 26 (1997) 203.
[7] (a) D. Gendron, M. Leclerc, Energy Environ. Sci. 4 (2011) 1225;
(b) Y. Zou, D. Gendron, R. Neagu-Plesu, M. Leclerc, Macromolecules 42 (2009) 6361;
(c) H. Bronstein, Z. Chen, R.S. Ashraf, W. Zhang, J. Du, J.R. Durrant, P. Shakya Tuladhar, K. Song, S.E. Watkins, Y. Geerts, M.M. Wienk, R.A.J. Janssen, T. Anthopoulos, H. Sirringhaus, M. Heeney, I. McCulloch, J. Am. Chem. Soc. 133 (2011) 3272;
(d) J.C. Bijleveld, V.S. Gevaerts, D. Di Nuzzo, M. Turbiez, S.G.J. Mathijssen, D.M. de Leeuw, M.M. Wienk, R.A. Janssen, J. Adv. Mater. 22 (2010) E242;
(e) M.-F. Falzon, A.P. Zoombelt, M.M. Wienk, R.A.J. Janssen, Phys. Chem. Chem. Phys. 13 (2011) 8931.
[8] (a) C. Kanimozhi, P. Balraju, G.D. Sharma, S. Patil, J. Phys. Chem. C 114 (2010) 3287;
(b) F.-L. Guo, S.-Y. Qu, W.-J. Wu, J. Li, W.-J. Ying, J.-L. Hua, Synth. Met. 160 (2010) 1767.
[9] S. Qu, W. Wu, J. Hua, C. Kong, Y. Long, H. Tian, J. Phys. Chem. C 114 (2010) 1343.
[10] J.E. Kroeze, N. Hirata, S. Koops, M.K. Nazeeruddin, L. Schmidt-Mende, M. GrÃ¤tzel, J.R. Durrant, J. Am. Chem. Soc. 128 (2006) 16376.
[11] D. Cao, Q. Liu, W. Zeng, S. Han, J. Peng, S. Liu, J. Polym. Sci. Part. A 44 (2006) 2395.
[12] E.Q. Guo, P.H. Ren, Y.L. Zhang, H.C. Zhang, W. Yang, J. Chem. Commun. (2009) 5859.
[13] G. Zhang, K. Liu, Y. Li, M. Yang, Polym. Int. 58 (2009) 665.
[14] Y. Zhu, A.R. Rabindranath, T. Beyerlein, B. Tieke, Macromolecules 40 (2007) 6981.
[15] A. Hagfeldt, M. Grätzel, Chem. Rev. 95 (1995) 49.
[16] M. Nazeeruddin, M. Grätzel, Transition metal complexes for photovoltaic and light emitting applications Photofunctional Transition Metal Complexes, vol. 123, Springer Berlin/Heidelberg, 2007, p. 113.
[17] T. Le Bahers, C. Adamo, I. Ciofini, J. Chem. Theory Comput. 7 (2011) 2498–2506.
[18] (a) S. Rühle, M. Greenshtein, S.G. Chen, A. Merson, H. Pizem, C.S. Sukenik, D. Cahen, A. Zaban, J. Phys. Chem. B 109 (2005) 18907;
(b) Y. Liang, B. Peng, J. Chen, J. Phys. Chem. C 114 (2010) 10992.
[19] S.A. Haque, E. Palomares, B.M. Cho, A.N.M. Green, N. Hirata, D.R. Klug, J.R. Durrant, J. Am. Chem. Soc. 127 (2005) 3456.
[20] J. Wiberg, T. Marinado, D.P. Hagberg, L. Sun, A. Hagfeldt, B. Albinsson, J. Phys. Chem. C 113 (2009) 3881.

[21] M.J. Frisch, et al., Gaussian 09 Revision A. 02, Gaussian Inc., Wallingford CT, 2009.
[22] (a) D. Jacquemin, E.A. Perpète, I. Ciofini, C. Adamo, Acc. Chem. Res. 42 (2009) 326;
(b) F. Labat, I. Ciofini, H.P. Hratchian, M.J. Frisch, K. Raghavachari, C. Adamo, J. Am. Chem. Soc. 131, (2009) 14290;
(c) M. Pastore, S. Fantacci, F. De Angelis, J. Phys. Chem. C 114, (2010) 22742;
(d) J. Preat, C. Michaux, D. Jacquemin, E.A. Perpète, J. Phys. Chem. C 113 (2009) 16821.
[23] J. Tomasi, B. Mennucci, R. Cammi, Chem. Rev. 105 (2005) 2999.
[24] C. Adamo, V. Barone, J. Chem. Phys. 110 (1999) 6158.
[25] T. Yanai, D.P. Tew, N.C. Handy, Chem. Phys. Lett. 393 (2004) 51.
[26] G. Scalmani, M.J. Frisch, B. Mennucci, J. Tomasi, R. Cammi, V. Barone, J. Chem. Phys. 124 (2006) 094107.